Since January 2020 Elsevier has created a COVID-19 resource centre with free information in English and Mandarin on the novel coronavirus COVID-19. The COVID-19 resource centre is hosted on Elsevier Connect, the company's public news and information website.

Building and Environment 183 (2020) 107206

Contents lists available at ScienceDirect

Building and Environment

journal homepage: http://www.elsevier.com/locate/buildenv

Evaluation of cough-jet effects on the transport characteristics of respiratory-induced contaminants in airline passengers' local environments

Yihuan Yan [a,b], Xueren Li [b], Lin Yang [b], Ping Yan [a], Jiyuan Tu [b,*]

[a] School of Air Transportation / Flying, Shanghai University of Engineering Science, Shanghai, 201620, China
[b] School of Engineering, RMIT University, PO Box 71, Bundoora, VIC, 3083, Australia

ARTICLE INFO

Keywords:
Cough-jets
Cough contaminants
Airliner cabin
Local environment
CFD
COVID-19

ABSTRACT

Urgent demands of assessing respiratory disease transmission in airliner cabins had awakened from the COVID-19 pandemics. This study numerically investigated the cough flow and its time-dependent jet-effects on the transport characteristics of respiratory-induced contaminants in passengers' local environments. Transient simulations were conducted in a three-row Boeing 737 cabin section, while respiratory contaminants (2 μm–1000 μm) were released by different passengers with and without coughing and were tracked by the Lagrangian approach. Outcomes revealed significant influences of cough-jets on passengers' local airflow field by breaking up the ascending passenger thermal plumes and inducing several local airflow recirculation in the front of passengers. Cough flow could be locked in the local environments (i.e. near and intermediate fields) of passengers. Results from comparative studies also revealed significant increases of residence times (up to 50%) and extended travel distances of contaminants up to 200 μm after considering cough flow, whereas contaminants travel displacements still remained similar. This was indicating more severe contaminate suspensions in passengers' local environments. The cough-jets was found having long and effective impacts on contaminants transport up to 4 s, which was 8 times longer than the duration of cough and contaminants release process (0.5 s). Also, comparing to the ventilated flow, cough flow had considerable impacts to a much wider size range of contaminants (up to 200 μm) due to its strong jet-effects.

1. Introduction

Global pandemics seem to become normalities in 2020. From the earlier 1918 Spanish flu to the latest Coronavirus diseases 2019 (COVID-19), the types and frequencies of the infectious diseases outbreaks have grown quickly and continuously been in the spotlight with equally familiar names as SARS, Swine Flu (H1N1), Ebola, Middle East Respiratory Syndrome (MERS), Zika, etc. [1,2]. The most recent outbreaks of COVID-19, caused by severe acute respiratory syndrome coronavirus 2 (SARS-CoV-2), has resulted in near 8 million people being infected with over 430,000 death reported worldwide [3]. Due to vastly increased imported cases of COVID-19 worldwide, many countries have locked down their cities with compulsory restriction measures (e.g. social distancing) [4], while thousands of airlines have halted their international and domestic services [5]. It appears that our collective vulnerability to the societal and economic impacts of the COVID-19 pandemic is inevitably increasing.

While the number of COVID-19 cases is still growing, the understanding of the transmission of COVID-19 virus also continues to improve [6]. The latest situation report from WHO revealed that the SARS-CoV-2 virus was mainly transmitted via exhaled droplets or by touching contaminated surfaces [6]. Human-to-human transmission of COVID-19 was summarised into three routes (Mittal et al., 2020): large expelled droplet directly acted on the recipients' mouth or nose; physical contact with the deposited droplets and subsequently transferred to respiratory mucosa; and aerosolised droplet nuclei from index patients' expiratory ejecta (i.e. aerosol transmission). Although the transmission model of COVID-19 seems to be similar to SARS, its basic reproduction number (R_0 up to 6.47) was found much higher than SARS (2.9) [7,8]. More devastatingly, the virus could be contagious during the asymptomatic incubation period [9]. Swab tests have detected higher viral load on the upper airways than throats of test patients with symptoms, and the viral load from asymptomatic carriers could be as high as that from symptomatic cases [10]. Since human respiratory activities, such as coughing, speaking and sneezing could release significant amounts of droplets and aerosols, these asymptomatic carriers could unknowingly

* Corresponding author. School of Engineering, RMIT University, PO Box 71, Bundoora, VIC, 3083, Australia.
E-mail address: jiyuan.tu@rmit.edu.au (J. Tu).

https://doi.org/10.1016/j.buildenv.2020.107206
Received 15 June 2020; Received in revised form 9 August 2020; Accepted 12 August 2020
Available online 16 August 2020

escalate the spread of pathogens through any respiratory aforementioned activities. The reveals on the transmission modes of COVID-19 virus well explained the reason why the number of imported cases vastly jumped in cruise ships and during long-distance flights. The enclosed environments with extremely high occupancy density became the perfect vessels for virus transmission in forms of droplets and aerosols [11,12]. Retrospective investigations of COVID-19 cases have found that more than 10% of passengers could be infected by the index patient during the flight [13,14]. As a result, the number of passengers that require quarantine was enormous and the economic burdens (frontline facilities, services, etc.) from these intensive quarantines were severe. At the moment, quarantine is still the only solution to the imported cases of communicable diseases from overseas. Therefore, deepened understandings of in-flight disease transmissions in associate with their transmission modes are urgently needed, which will be the vital key leading to a more effective quarantine strategy after landing.

With the unique airliner cabin environments being widely reported (i.e. high occupancy density and limited confined space), many important design parameters and factors such as the thermal comfort of passengers [15,16], ventilation scheme [17,18], seats arraignment [19] and passengers' body heat [20,21] have been carefully investigated in existing literature. Among these factors, the release location of contaminants and corresponding seats arrangements were found having substantial impacts on contaminants distribution [11,19], while the thermal plume induced by passengers' body heat could significantly influence the contaminants transport by elevating the contaminants upward with the ascending thermal plume [20]. Also, as reported in several studies [22,23], the movement of passengers and cabin crews could stimulate contaminants to transport further across the cabin. These studies provided deepened understandings on the transport characteristics of contaminants in airliner cabin environments and successfully narrowed down the list of main affecting factors. However, one of the most critical factors, the release process of contaminants, were overlooked in most existing studies due to various reasons. Experimentally, it was extremely challenging to add additional contaminants generator and sourcing tubes into already crowded cabin mockup to restore the real contaminants release process from human sources. These devices could be obstacles occupying vital spaces in front of passengers and would lead to inaccurate local measurement of airflow distribution. Although numerical approach could be more favorable to imitate the real contaminants release process, it was still either completely neglected or simplified as constant release in many existing studies [20,24]. This was mainly because that modelling contaminants transport in multi-coupled and multi-scale cabin domains requires significantly high computational cost and thereby the instantaneous release details of contaminants were compromised. However, this overlooked factor could be a vital gap when investigating respiratory disease transmission (e.g. COVID-19) in airliner cabins.

When respiratory disease viruses (e.g. SARS-CoV-2) are released from the host in forms of droplets or aerosols by coughing or sneezing, these respiratory activities may also have significant influences on the local-environment around occupants and affect the transport characteristics of released droplets. Existing studies found that cough in a confined space could cause turbulent jets with Reynolds number of 10^4 and generate so-called 'cough-jet' immediately after release [25]. The strong cough-jet with high-velocity airflow could induce instability in the local airflow interface and could even have a significant impact on the neighbours' breathing zones [26]. Kwon et al.'s experimental measurements in an occupant's breathing zone also captured significant interference of local airflow by coughing and speaking jets [27]. The importance of jet flow from respiratory activities have been well recognised through existing studies in traditional enclosed spaces, however, its significance in a more extreme enclosed space, the airliner cabin, is still underrated. Existing studies by Gupta et al. [12] in an airliner cabin reported that cough-jet should be one of the primary factors in the airborne disease transmission since peak concentration of contaminants

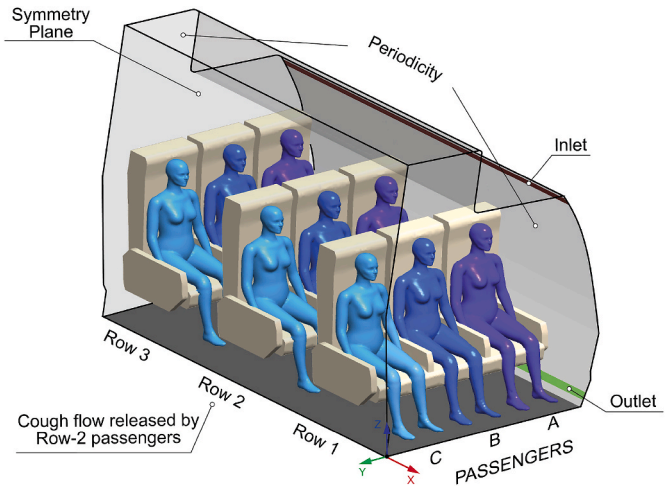

Fig. 1. Computational model of cabin section and passengers.

immediately occurred after release and were dominated by cough-jet. Their study revealed strong necessity of including the instantaneous release process of contaminants via respiratory activities. However, due to the limits of computational capacity at early stage, the passenger models in their study were over-simplified using regular blocks. It was a commonly applied approach to reduce computational cost, until recent studies found that over-simplifying manikin models could induce dead flow zones in the vicinity of manikin and would cause inaccurate airflow pattern and contaminants concentration predictions in the micro-environment of occupants [28]. These drawbacks from over-simplification could be further enlarged in cabin environments due to extremely large number of passengers sitting closely. Therefore, it is worth the efforts of applying manikin models with real human body features when investigating the instantaneous release process of airborne disease and its transmission in passengers' local environment. Also, due to the high occupancy density and narrowed sitting space in airliner cabins, each row of passengers sitting closely to each other could form their own enlarged local environments and the entire cabin environment is mainly composed of many local environments. However, whether the enlarged passengers' local environments could extend the duration of cough-jet effects or even promote the transmission of airborne disease still remain unknown. These findings would be of great interests to airliner manufacturers for new ventilation designs and optimisations. Therefore, it is essential to understand the interactions between respiratory-induced jet flow and contaminants transport in passengers' local environments.

Therefore, with the urgent need of assessing respiratory disease transmission in airliner cabins being awakened from COVID-19 pandemics, this study carefully investigated one of the critical but long overlooked factors, the instantaneous release process of respiratory-induced contaminants. Coughing, one of the most common respiratory activities, was modelled in a three-row cabin of Boeing 737 to study the impacts of cough-jet flow on the airflow field and contaminants transport in the local environment of passengers. Cough contaminants were released with the jet flow from various passengers at different locations, and the release processes were modelled using transient Eulerian-Lagrangian approach. Dominating parameters on contaminants transmission, such as the cough flow field, droplets travel distance and size distributions were carefully studied.

2. Method

2.1. Computational models

An economy cabin section was built based on one of the widely

served medium-size commercial aircrafts Boeing 737, as illustrated in Fig. 1. Since the focus of this study was on the local environment of passengers (i.e. the region in the vicinity of seated passengers at the same row), a three-row cabin section was found sufficient to capture the instantaneous developments of cough flow and contaminants release process from passengers sitting in the second row. The distanced travel of contaminants in a full-size economy cabin was not considered in this study. The ventilation inlets and outlets were located on the side of cabin, as demonstrated in Fig. 1. Due to symmetric 3 by 3 seats arrangement and ventilation design in the economy cabin, half of the cabin section including 9 computational thermal manikins (CTMs) and seats was modelled to save the computational cost. All CTMs used in this study contain real human body proportions and detailed body features, since over-simplifying CTMs could lead to inaccurate predictions of human local environment [28]. These CTMs were firstly obtained from 3D scans and were further optimised in our previous study [29] to achieve well balanced computational cost and accuracy.

The cabin domain and CTMs were discretised using unstructured tetrahedron mesh. Local mesh refinement was applied in the front of sitting CTMs, while 10 prism layers with total height of 15 mm were created on each CTM's surfaces to capture gradient changes of local velocity, temperature, etc. Mesh independency test was conducted using the y + values at CTM surfaces [30] and the grid convergence index (GCI) [31] among four sets of mesh. Mesh independency was achieved when the total mesh element number reached 3.5 million with 90% mesh quality above 0.78 and the maximum y + values below 3 at all CTM surfaces. Further mesh refinement (approx. 5 million) only contributed less than 5% improvements.

2.2. Mathematical models

The airflow field in the cabin domain was solved using the incompressible Navier-Stokes equations with the Boussinesq approximation for the thermal buoyance flows. High-resolution advection scheme was applied to achieve better robustness and accuracy of the advection terms, while the SIMPLEC algorithm was employed for the velocity-pressure coupling. RNG k-ϵ model obtained high reputation on predicting indoor airflows [32], although it might overestimate contaminants deposition. This study employed RNG k-ϵ model for modelling the turbulence in airflow field considering its successful applications in the past studies [33]. The contaminants transport and their trajectories were tracked using the Lagrangian framework. Significant forces including the drag force $\vec{F}_d$, the buoyance force $\vec{F}_{bouy}$ and the virtual mass force $\vec{F}_{v.m}$ were considered and expressed in Equations (2) – (4).

$$m_p\frac{d\vec{U_p}}{dt}=\vec{F_d}+\vec{F}_{bouy}+\vec{F}_{v.m.} \tag{1}$$

$$\vec{F}_d=\frac{C_D}{2}\frac{\pi d_p^2}{4}\rho_a\left|\vec{U}_p-\vec{U}\right|\left(\vec{U}_p-\vec{U}\right) \tag{2}$$

$$\vec{F}_{\text{bouy}}=\frac{\pi d_p^3}{6}(\rho_p-\rho)\text{g} \tag{3}$$

$$\vec{F}_{v.m}=\frac{C_{v.m.}}{2}\frac{\pi d_p^3}{6}\left(\frac{d\vec{U_P}}{dt}-\frac{d\vec{U}}{dt}\right) \tag{4}$$

Since the cabin environment has relatively low velocity and high turbulence [34], the dispersion of aerosol contaminants is mainly dominated by the fluctuating component of airflow. In Lagrangian framework, the turbulent dispersion of contaminants was modelled by adding an eddy fluctuating component to the mean air velocity in association with the entering contaminants. The local air velocity is redefined in Equation (5).

$$\vec{U}=\bar{U}+U' \tag{5}$$

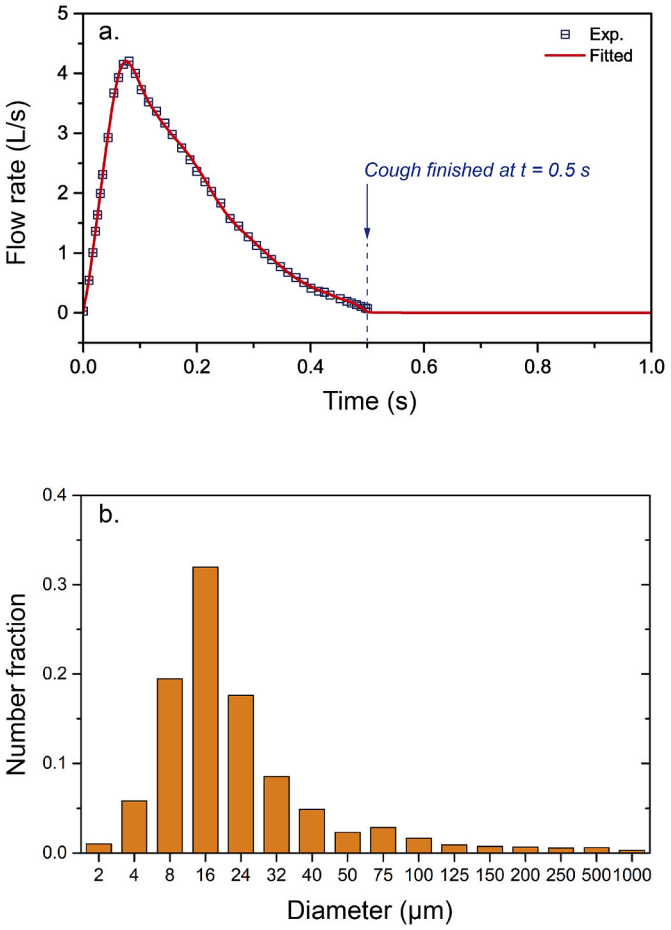

Fig. 2. Cough flow and contaminants release conditions; a. flow rate of single cough and b. Size distribution of contaminants.

$$U'=\varphi\left(\frac{2k}{3}\right)^{0.5} \tag{6}$$

where $\bar{U}$ is the mean air velocity, U' is the fluctuating eddy velocity and φ is a normal distributed random number which accounts the randomness of turbulence by a mean value.

In each eddy, the fluctuating eddy velocity is varied by the lifetime t_e and the length L_e of the eddy, as expressed in Equations (7) and (8).

$$L_e=\frac{C_\mu^{3/4}k^{3/2}}{e} \tag{7}$$

$$t_e=\frac{L_e}{\left(\frac{2k}{3}\right)^{1/2}} \tag{8}$$

where C_μ is the turbulent constant, k and ϵ are the local turbulent kinetic energy and dissipation, respectively.

2.3. Boundary conditions and numerical setup

The ventilated flow rate inside the cabin was set according to the American Society of Heating, Refrigerating and Air-Condition Engineering (ASHRAE) aviation standard [35]. Based on ASHRAE standard, a minimum air supply of 9.4 L/s per person was required and thereby an equivalent air mass flow rate of 0.04 kg/s was set at the inlet with air temperature of 20 °C. The convective heat load of each CTM was set at 36 W based on existing experimental measurements [36,37], which was

Table 1
Contaminants size and number distributions.

Diameter (μm)	2	4	8	16	24	32	40	50
Number	51	291	974	1598	879	427	245	116
Diameter (μm)	75	100	125	150	200	250	500	1000
Number	143	83	46	38	34	29	31	15

Table 2
List of case studies.

	Released by passenger A (row-2)	Released by passenger B (row-2)	Released by passenger C (row-2)
With cough flow	Case 1	Case 2	Case 3
Without cough flow	Case 4	Case 5	Case 6

in equivalent to the heat flux of 22.8 W/m^2. The radiative heat load was not considered in this study. As illustrated in Fig. 1, the front and back planes of the cabin section were set as translational periodicity. This would allow airflow to leave and re-enter the domain more freely with a periodic pattern and could avoid unreal flow recirculation or dead zones near the front and back boundaries. Also, a symmetry plane was set at the middle of the aisle since the airflow pattern was found approximately symmetric on each side of the aisle in existing literature [24,34]. Other solid surfaces including floor, seats and ceiling were considered as adiabatic.

Cough flow was released from passengers sitting at the second row, while only one passenger was coughing each time. Considering the mouth profile of the CTM was based on real human mouth that is not a perfect circle, an equivalent mouth opening of approximately 3 cm in diameter was used. Since the flow rate of single cough was not consistent over time, the time-dependent cough flow rate was set based on existing experimental coughing measurements [38], as illustrated in Fig. 2a. Contaminants were expelled simultaneously with the cough-jet from each passenger's mouth. Since the size of droplets released by cough dispersed diversely, a full-size range of contaminants (from 2 μm to 1000 μm) was included in this study. The contaminants size distribution and number fraction of each size group were set according to existing experimental measurement from real coughs [25], as demonstrated in Fig. 2b. The evaporation process was not considered in this study. The Lagrangian particle tracking model was employed to continuously trace the motions of contaminants, while 5000 trajectories were found sufficient to achieve consistent contaminants concentration in this three-row cabin domain. Detailed number of trajectories for each contaminant size

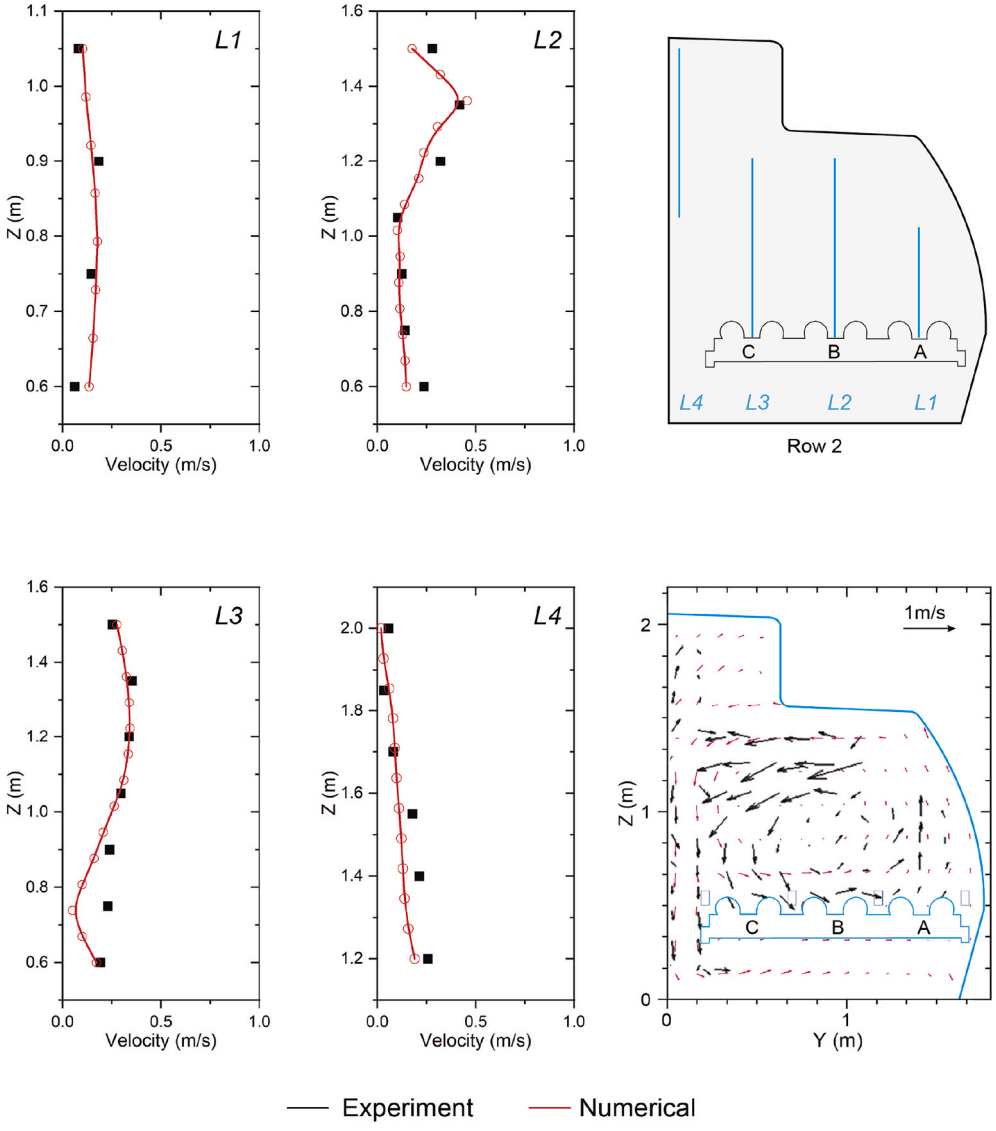

Fig. 3. Velocity validation at selected lines and plane.

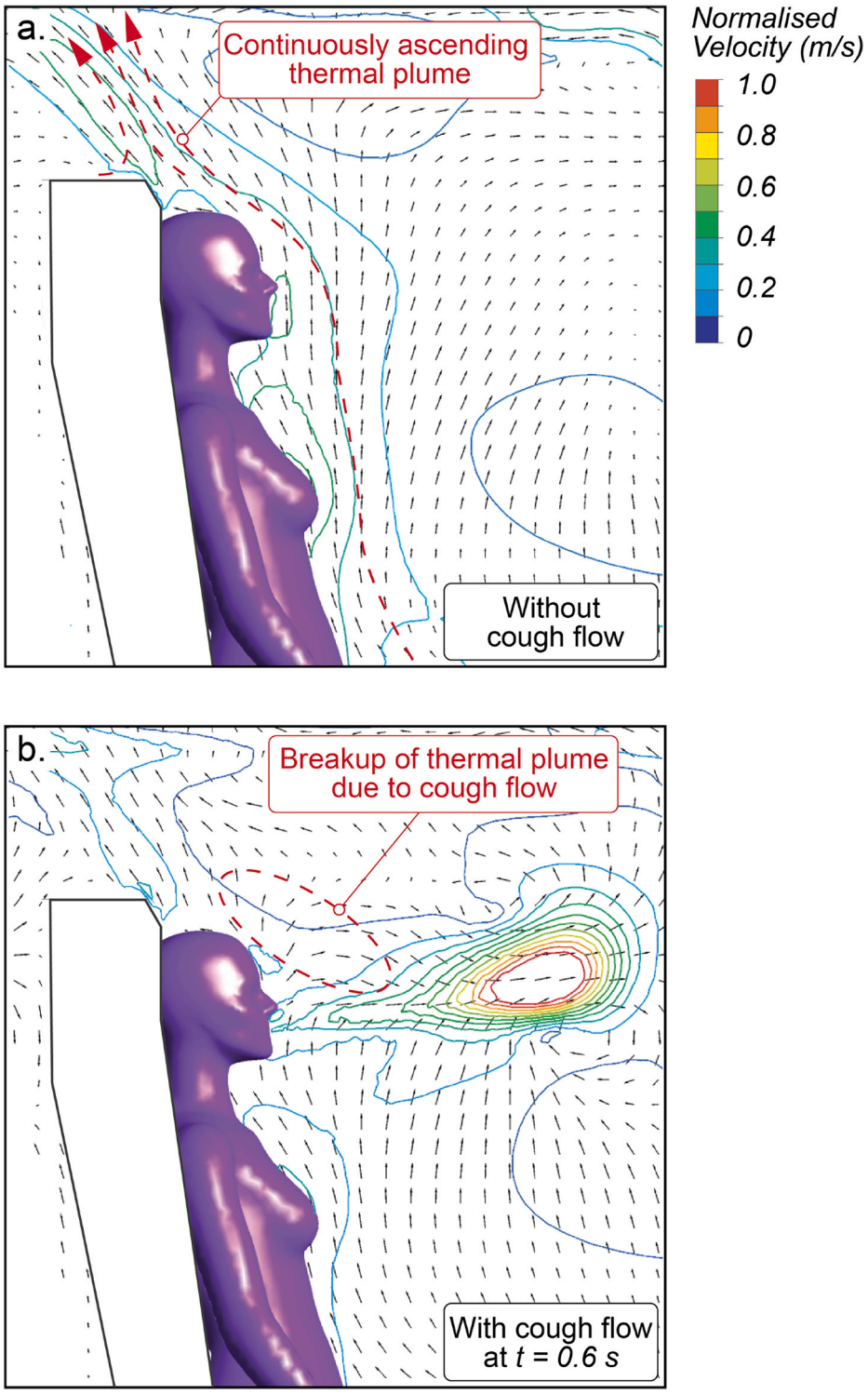

Fig. 4. Comparisons of airflow distribution; a. Without cough flow, b. With cough flow at $t = 0.6$ *s*.

was set accordingly to its number fraction and was listed in Table 1. Contaminants were assumed to be fully deposited when hitting walls (floors, seats, cabin walls, etc.) due to the factor that real cabin materials are highly absorptive (e.g. wool or nylon carpet, leather upholstery and fabric).

Transient simulations were conducted with adaptive time steps to capture the simultaneous development of cough flow and contaminants release process. Single cough behaviour was simulated each time by applying one pulse air jet with duration of 0.5 s. Very small initial time-steps of 0.01 s were used at the beginning of the cough process with maximum increase ratio of 1.1. The total tracking time was 10 s, which took over 25 h to finish each simulation using a workstation with 40 CPU cores (2.8G Hz Intel Xeon) and 128 GB RAM. Three cases with cough flow were studies, in which Passenger A (window seat), B (in the middle) and C (aisle seat) at the second row was coughing in each case, respectively. In addition, another three cases were simulated without considering the cough flow, while contaminants were still released by same passengers via the mouth. Contaminants in these cases were

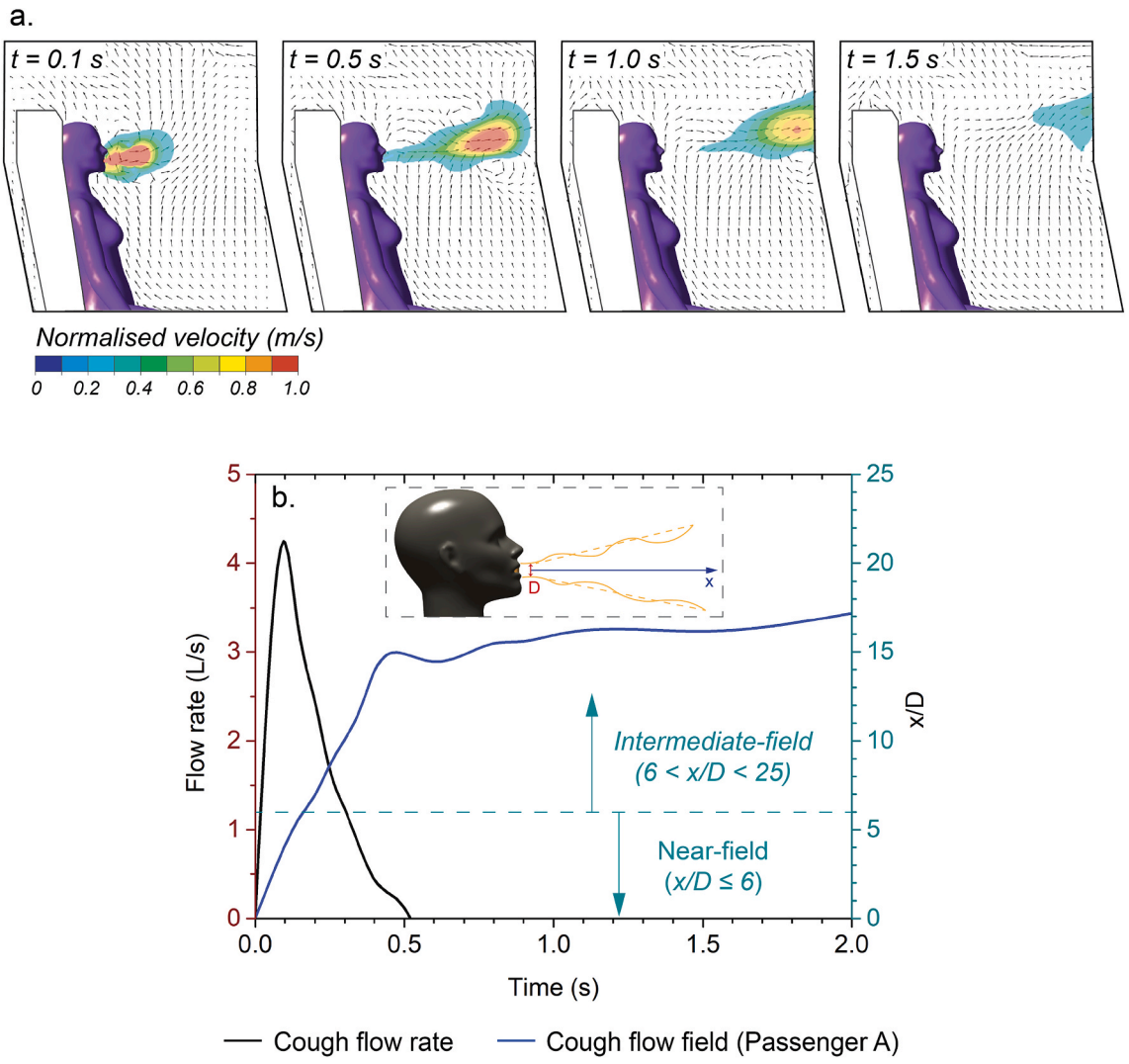

Fig. 5. Cough flow by Passenger A; a. Cough flow development, b. Cough flow field over time.

released with initial velocity of 1 m/s, while their release locations, numbers and size distributions remained same as the cough cases. Therefore, a total of six cases were presented and compared in this study as listed in Table 2.

3. Results and discussion

3.1. Airflow field and cough-jet

Before considering the cough flow from passengers, the predicted airflow field was firstly compared to experimental measurements by Li et al. [18] for model validation. In their experimental study, detailed velocity profiles were measured at various locations using particle image velocimetry (PIV) in a Boeing 737 mockup. Identical locations including a two-dimensional plan in front of row-2 passengers and four vertical lines were selected in this study to compare the airflow distribution and local velocity profiles, as illustrated in Fig. 3. The velocity vectors predicted in this study yielded very similar airflow directions and 2D airflow distributions to the experimental measurements in most regions of the selected plane. Both experimental and numerical results revealed a dominating counter-clockwise airflow circulation in the left-side cabin domain. An opposite clockwise airflow circulation was also captured by Li et al. on the other side (right) of the cabin, which proved the approximate symmetry characteristics of airflow distribution in cabin due to symmetrical ventilation design and seats arrangement. Slight deviations were found near the edges of the PIV measurements, such as the airflow direction near the ground level. Further quantitative comparisons of local velocity profiles were conducted along four vertical lines, in which three of them were in front of sitting passengers, as demonstrated in Fig. 3. The predicted local velocity profiles at selected lines yielded very similar pattern to the experimental measurements. Although slight deviations were noticed at some sample points between the numerical and experimental results, most of these points were near the boundaries (e.g. the floor and the ceiling) of PIV measurements. Overall, the local velocity profiles from this study well agreed with Li et al.'s experimental measurements.

To study the cough-jet effects, the airflow distributions in passengers' local environments were firstly compared with and without considering the cough flow. Detailed comparisons of velocity vectors and contours in passenger A's micro-environment was demonstrated in Fig. 4. A continuous and strong ascending thermal plume can be clearly observed from Fig. 4a before considering the cough flow. The maximum velocity of ascending thermal plume (approx. 0.4 m/s) from passengers in cabin environment was found slightly higher than traditional indoor spaces with single sitting person (approx. 0.3 m/s) [28]. This enlarged thermal plume was mainly induced by closely sat passengers with merged heat loads and limited spaces above passengers. Although passenger's thermal plume became stronger in cabin environment, it was

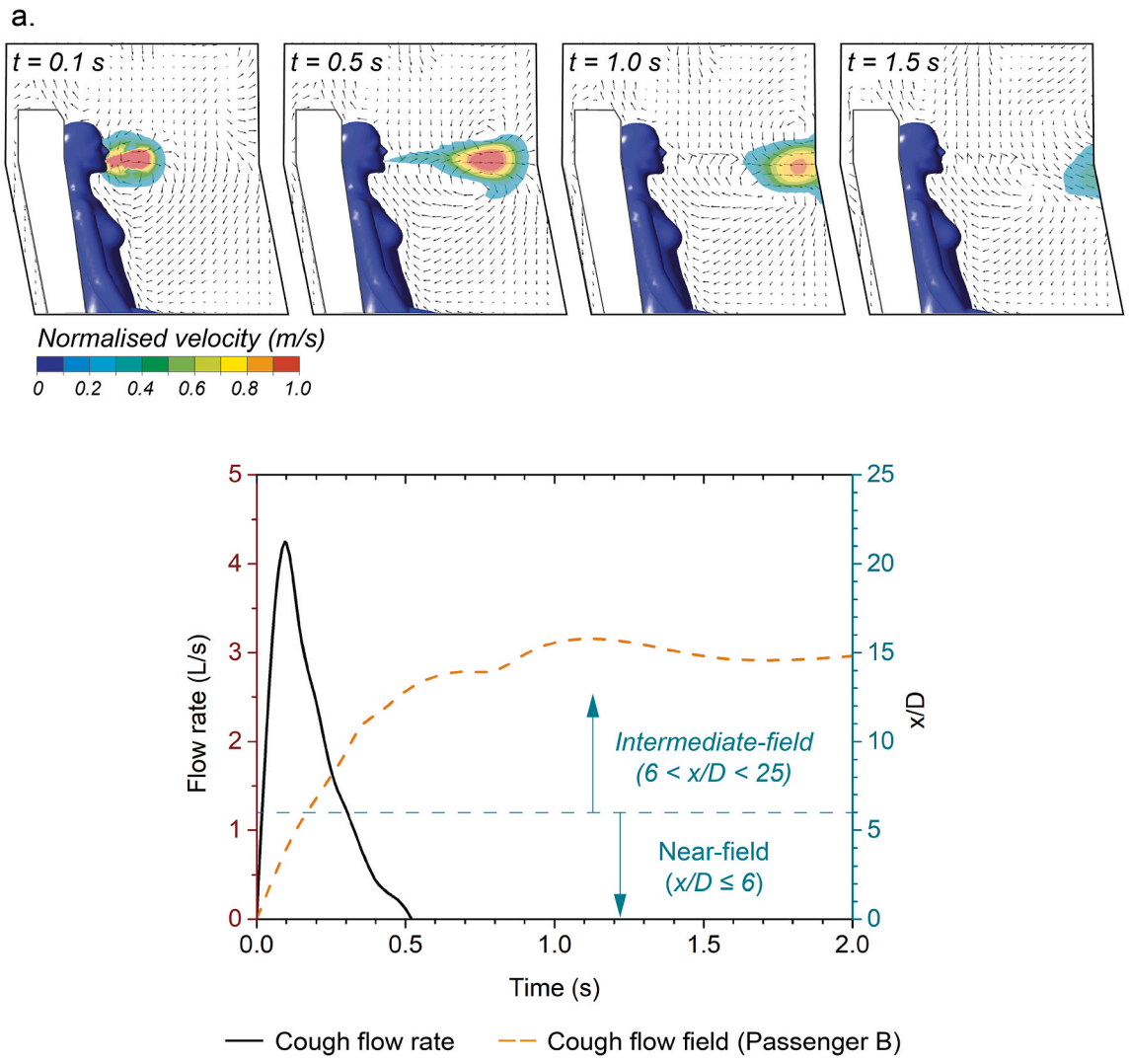

Fig. 6. Cough flow by Passenger B; a. Cough flow development, b. Cough flow field over time.

still affected by the cough-jet after considering the cough flow. Fig. 4b showed the local airflow distribution immediately after cough at t = 0.6 s, in which the ascending thermal plume was clearly interrupted by the cough flow above passenger A's breathing region and led to a relatively weaker ascending thermal plume above passenger's head. Due to the breakup of thermal plume and the strong effects of the cough-jet, local airflow recirculation was observed in front of the sitting passenger. Since the airflow was relatively quiescent in passenger A's local environment, the effects of the cough-jet were significant and was suspected to last much longer after the completion of coughing behaviour.

To identify the effective duration of cough flow and its continuous influences on passenger's local environment, detailed development of cough flow by passenger A was analysed at various time steps, as demonstrated in Fig. 5a. It can be noticed that the cough flow was quickly developed during the cough process (up to 0.5 s) and formed a strong cough-jet breaking up the local airflow field. This cough-jet continued to travel further even after the cough was finished and gradually dispersed over time. The ratio of cough flow distance (x) and the mouth opening diameter (D) was then plotted in Fig. 5b to reflect the coverage of cough flow over time. The x to D ratio was used to identify whether the cough flow was in the local environment of passengers. According to Fellouah et al.'s measurements [39], a near-field is defined with the x to D ratio up to 6, while an intermediate-field can be defined with x/D ranged from 6 to 25. A far-field is defined when the ratio of cough flow distance and mouth opening diameter becomes larger than 25. The near-field represented the region in the vicinity of the occupant, while the intermediate-field could still be considered in the local environment of sitting occupants. It is worth noting that the equivalent 3 cm mouth opening diameter based on the employed CTM in this study was higher than the measured mouth opening during coughs (2 ± 0.5 cm) [40,41]. This might cause underestimations of the normalised distance (i.e. x/D). As shown in Fig. 5b, the cough-jet quickly passed the near-field in approximately 0.2 s even before the cough release process was completed. However, the cough-jet was fluctuating at x/D around 10 to 15, which indicated that the cough-jet was unable to leave the passenger's local environment or traveled further to the far-field. In this case when passenger A was the focus, this trapped cough-jet could be due to the limited upper space above passenger A or the narrow space of each row in economy cabins.

To evaluate whether the sitting location could affect the coverage of cough flow, coughs released by passengers B and C were further studied. The time dependent development of cough flow and its coverage field were plotted in Figs. 6 and 7. The cough released by passenger B (Fig. 6a) showed a similar development pattern to that of passenger A. On the other hand, it was noticed from Fig. 7a that the cough flow released by passenger C had more interaction with the local airflow. This was indicating that the ventilated air supply was much stronger near passenger C. Also, the aforementioned counter-clockwise air

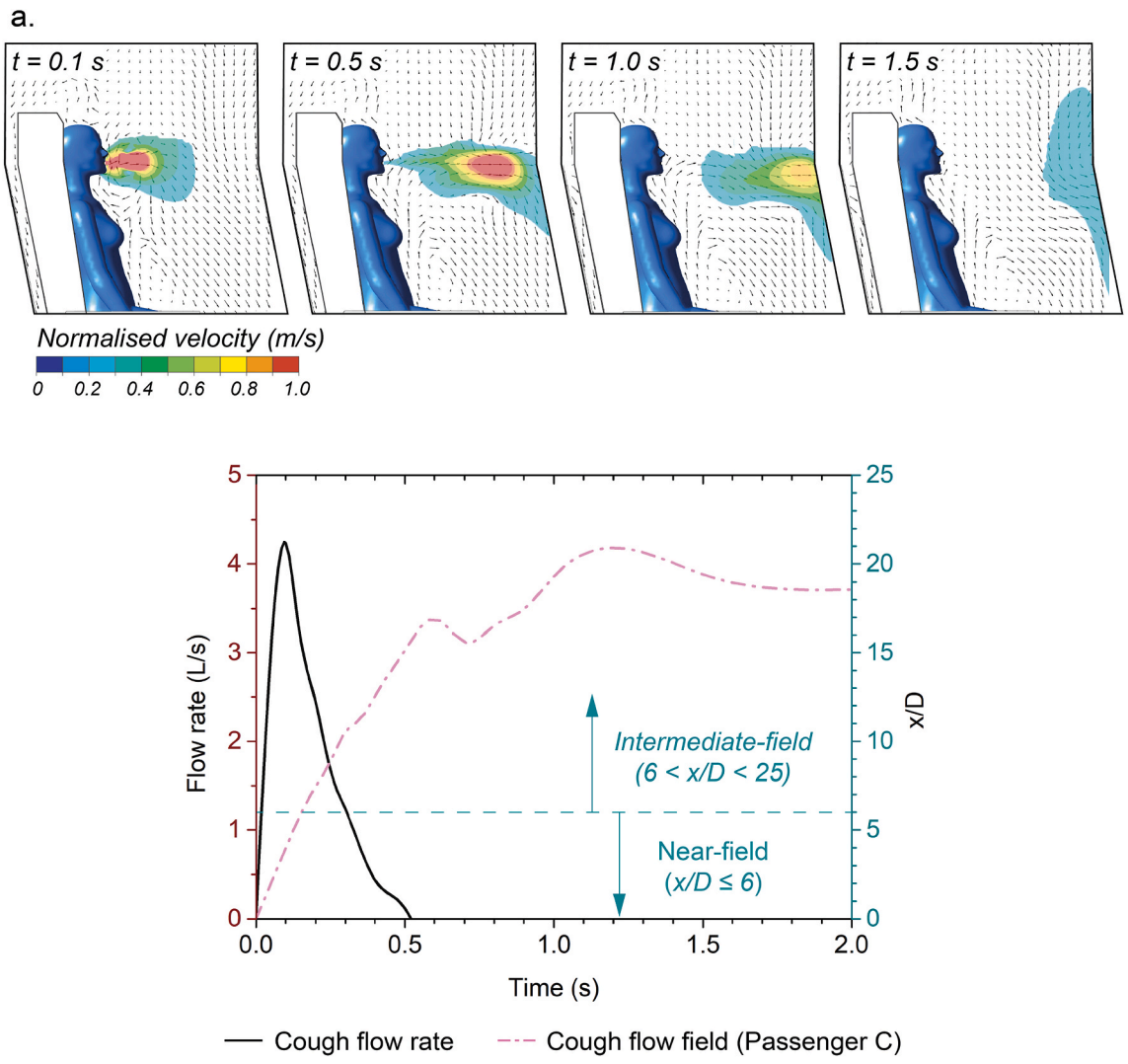

Fig. 7. Cough flow by Passenger C; a. Cough flow development, b. Cough flow field over time.

recirculation was contributing significant downward airstream near the location of passenger C. As a result, the cough flow traveled further downward and dispersed wider over time. In terms of the cough flow field, the x/D from passenger B's cough yielded very similar profile to that from passenger A. Although the ratio of cough flow distance and mouth opening was slightly higher in the case when passenger C was coughing, it was still under the range of intermediate-field. Therefore, the cough flow was found easily trapped in the local environment of passengers, regardless of their sitting locations. It was concluded that the narrow sitting space in this economy cabin could be the main cause to the trap of cough flow. Once the cough flow stayed longer in passengers' local environment, it could generate several local airflow recirculation and potentially lead to longer suspension time of released respiratory contaminants.

3.2. Effects of cough-jet on contaminants transport

Contaminants were released with the cough process during the first 0.5 s. The cough contaminants transport characteristics were firstly compared among three cases (cases 1, 2 and 3), in which each of passenger in the second row was coughing.

Fig. 8 showed the predicted trajectories of contaminants from four size groups (i.e. 0 – 10 μm, 10–50 μm, 50–100 μm, and >100 μm). It was noticed that the transport of smaller contaminants (below 50 μm) was jointly dominated by the cough-jet and ventilated airflow. These small contaminants were quickly ejected horizontally due to the strong jet effects of cough flow. Meanwhile, due to insignificant weight of small contaminants, the vertical travel of these small contaminants heavily relied on the local ventilated flow (i.e. the counter-clockwise air recirculation). As a result, small contaminants released by passenger A was travelling with higher upward components, whereas same groups of

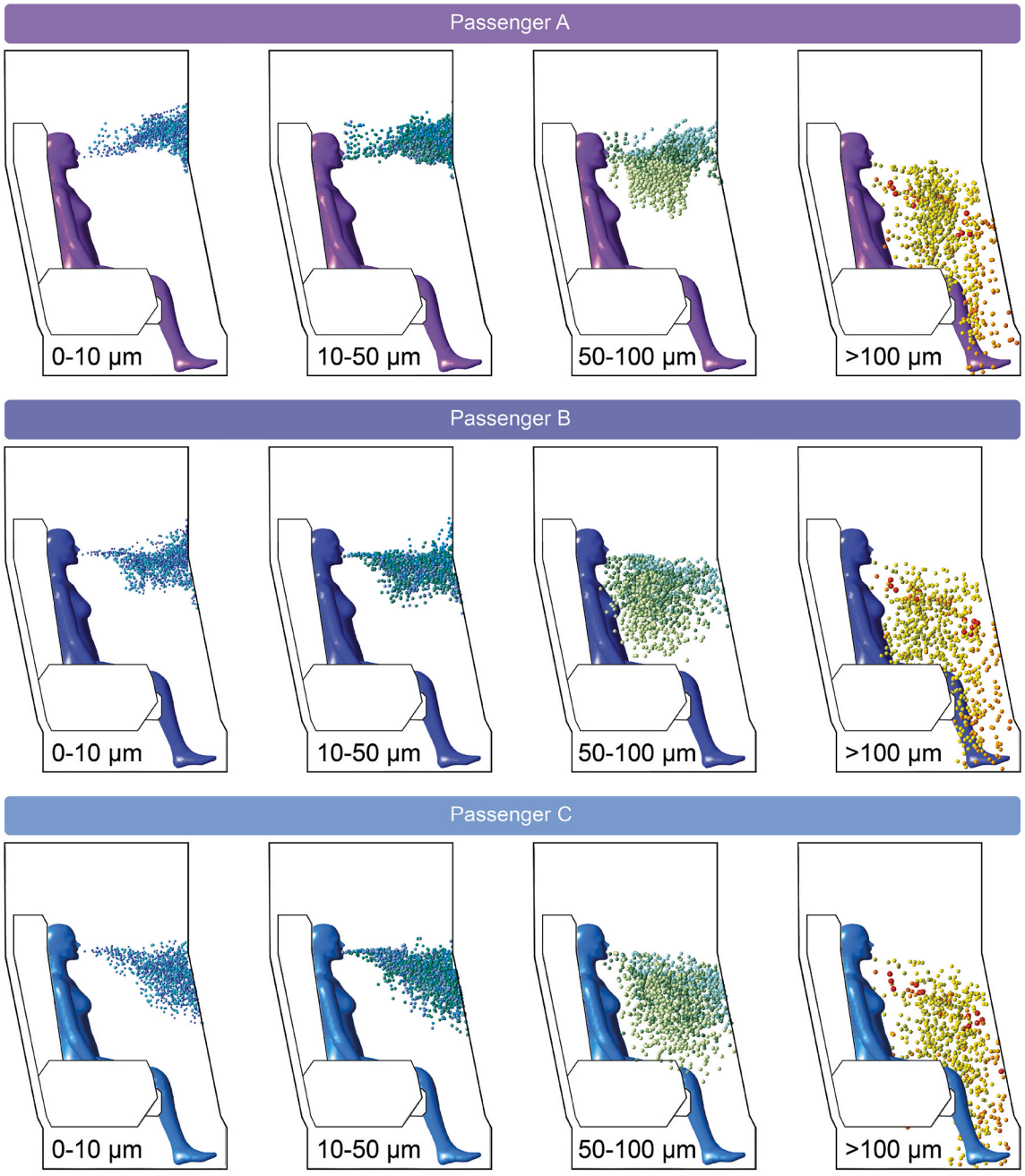

Fig. 8. Contaminants trajectories after release by passengers at t = 1.5 s.

contaminants tended to travel further downward when passenger C was coughing. While the cough-jet effect remained significant on contaminants sizing from 50 μm to 100 μm, the ventilated flow started to loss its dominating effects on this size group due to increased weight and inertia of larger contaminants. For large contaminants (>100 μm), the cough-jet still had effect on the contaminants transport although it was clearly weakened. On the other hand, the impacts from ventilated flow was almost neglectable as contaminants were settling down significantly

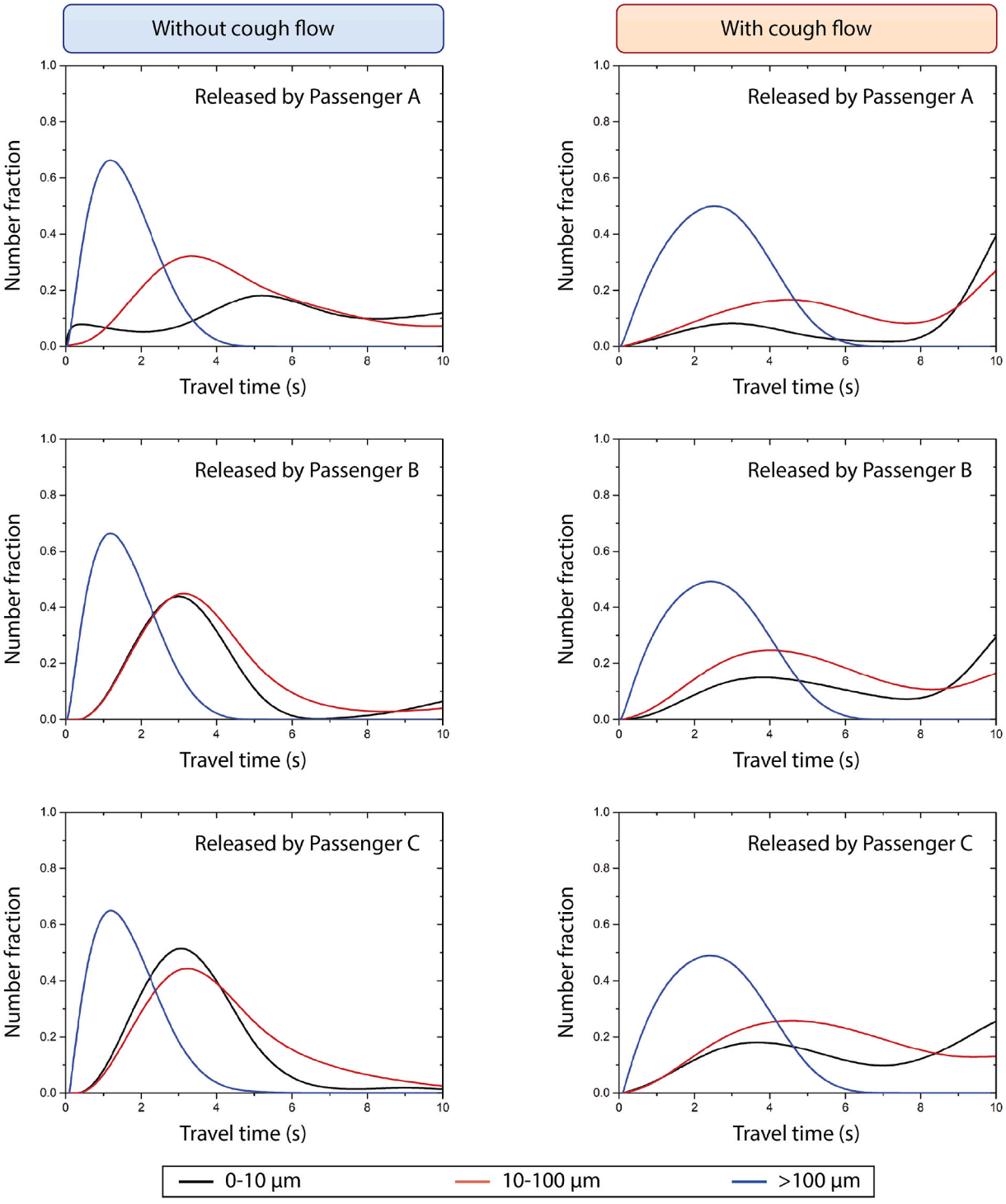

Fig. 9. Contaminants number fraction distribution in the air.

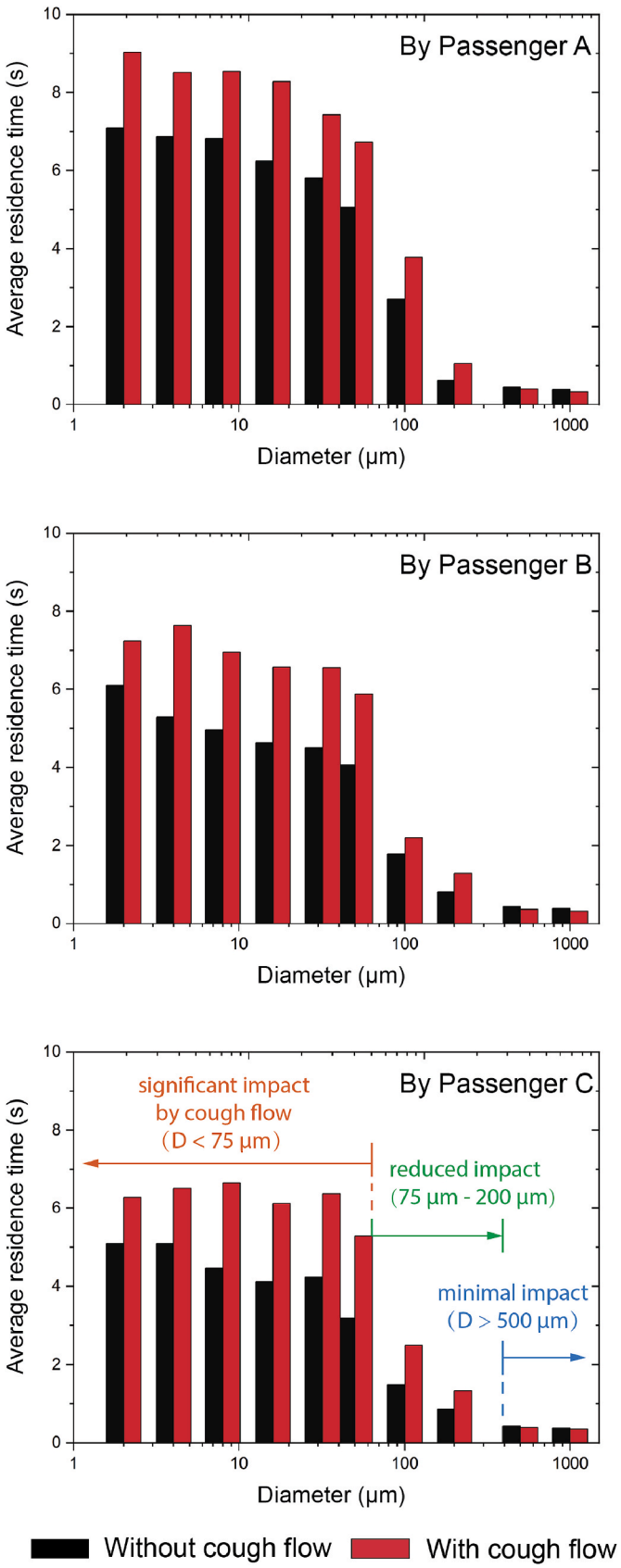

Fig. 10. Comparison of average residence time before and after considering cough flow.

due to weight.

With the effects of cough-jet on contaminants trajectories being clearly visualised, the travel time of contaminants were further compared with and without considering the cough flow. Fig. 9 plotted the travel time of contaminants against their number fractions in each size group. It was clearly observed through comparisons that the peak of number fractions from all three size groups were clearly delayed after considering the cough flow, which indicated longer contaminants travel time. Specifically, the cough-jet had strongest effects on extending travel time of contaminants below 10 μm, in which most of contaminants were travelling longer than 10 s with cough flow. A similar pattern was also found on contaminants between 10 and 100 μm, in which the cough-jet stimulated higher fraction of contaminants to travel longer than that without cough flow. Although the cough-jet effects were found less significant to the large size group (>100 μm) comparing to the other two groups, the maximum travel time was still considerably increased nearly 50% after considering the cough flow. It was also an interesting finding that contaminants released by passenger A revealed different travel time pattern than those from passengers B and C in the cases without cough flow. This was mainly due to the factor that the local airflow was relatively quiescent near the window seat passenger and thereby small contaminants would suspend longer in the air. However, after considering the cough flow, the jet effects from cough was more significant than the local ventilated airflow and eventually led to a similar travel time pattern of contaminants released by different passengers.

The average residence time of each contaminant size in the air was further compared, as shown in Fig. 10. For extremely small contaminants, the increase of residence time after considering cough flow was not dramatic. This was because that the ventilated flow had already caused long residence time of these contaminants due to their extremely small weight and inertia. However, for larger contaminants (e.g. 50 μm, 75 μm and 100 μm) with considerably increased weight and inertia, the influences from ventilated flow were very minimal, whilst the impacts from cough-jets became more obvious and led to a significant increase of residence time on these contaminants with cough flow. The cough-jet was found having significant impacts to contaminants up to 100 μm, these impacts gradually reduced with the further increase of contaminant size and became minimal with contaminants larger than 500 μm. Therefore, comparing the ventilated flow, the cough flow could have considerable impacts to a larger size range of contaminants up to 200 μm. Also, the average residence time of contaminants released by passenger A was higher than the other two cases, although the travel time pattern became similar after considering the cough flow. On other words, contaminants could suspend longer in the local environment of window seat passengers who had even less space than middle and aisle passengers.

To better understand the causes of longer residence time after considering the cough flow, the travel motion characteristics of each contaminant size were compared with and without cough flow. Fig. 11a illustrated the travel distance (D) versus displacement (d) before and after considering the cough flow from passenger A. It can be clearly noticed that the travel displacement was almost the same with and without the cough flow, which indicated that the contaminants did not travel further away from passengers. However, by looking into the distance comparisons, significant increases of distance were observed on contaminants up to 200 μm with cough flow. Also, the difference between the displacement and distance was further enlarged because of the cough-jet, which indicated increases of contaminants suspensions and recirculation in the local environment of passengers. The ratio of distance (D) and displacement (d) at each contaminant size was then shown in Fig. 11b. Contaminants suspension was not significant without the cough flow, as the local environment of passenger A was relatively quiescent. On the other hand, when contaminants were released with cough flow, severe suspensions were found at contaminants up to 100 μm with travel distance more than doubled than the displacement. Therefore, comparing to the ventilated flow, the cough-jets could have

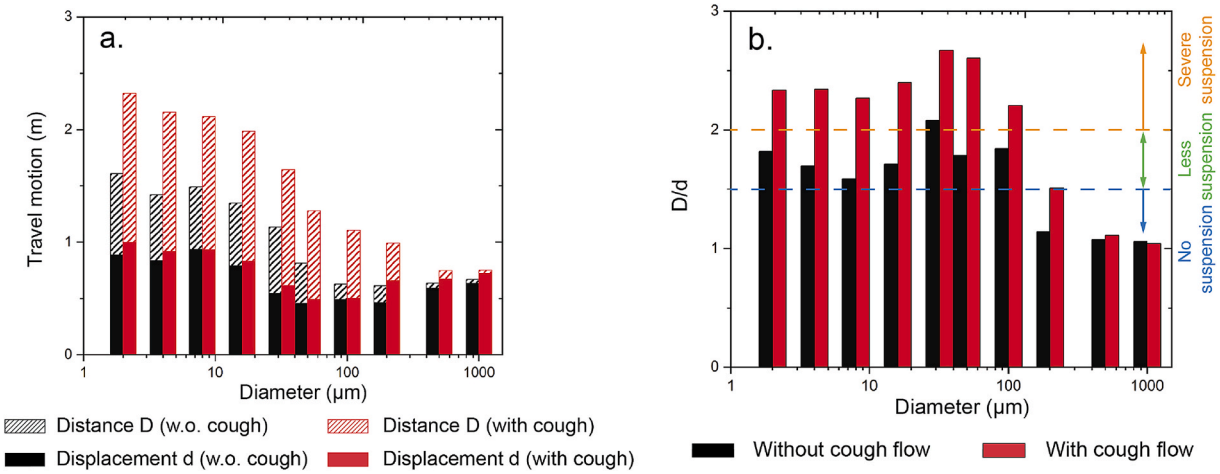

Fig. 11. Comparison of contaminants motions (from passenger A) with and without cough flow; a. Travel distance D v.s. Travel displacement d, b. Ratio of distance to displacement.

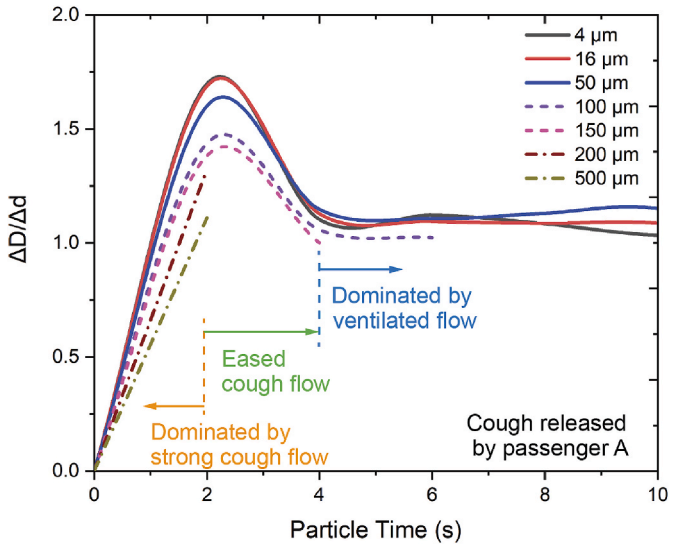

Fig. 12. Cough flow impacts on contaminants transport over time (from passenger A).

considerable impacts on a much wider size range of contaminants (up to 200 μm).

Also, the effective duration of the cough-jets could be essential on the transport characteristics of cough contaminants. The above outcomes had revealed a stronger impact of cough-jets on contaminants travel distances than that on contaminants travel displacements. Therefore, the ratio of travel distance intervals to displacement intervals over time could be a clear indicator when the cough-jets were having significant impacts on the contaminants field. Seven sizes of contaminants from 4 μm to 500 μm were plotted in Fig. 12 for comparisons. The ratios of travel distance intervals to displacement intervals were sharply increased during the cough process (0.5 s) and 1.5 s after the completion of cough process. These dramatic ratio increases indicated a dominating impact from strong cough flow on the transport characteristics of all sizes of cough contaminants. The cough-jets effect was found eased in the next 2 s (up to t = 4 s) with the plotted ratios gradually reduced. The ventilated flow took over and dominated flow after 4 s when the cough-jets were almost fully dispersed. Also, the results showed that small contaminants had higher ratio of travel distance to displacement intervals than the large ones in the first 4 s, which revealed more suspensions from small cough contaminants. Overall, the effective cough-jets could last at least 4 s in passengers' local environment and could affect the transport characteristics of contaminants up to 150 μm during the entire period.

4. Conclusion

The time-dependent cough flow and contaminants released from passengers sitting at the window seat, in the middle and at the aisle seat in a medium-size economy cabin section were investigated in this study. The effects of cough-jet in passengers' local environments were focused, while the cough-jets impacts on local airflow field and instantaneous cough contaminants transport characteristics were carefully evaluated. Outcomes from this study were concluded as follows:

(1) The cough flow could severely break up the ascending thermal plume of seated passengers, even though the thermal plume became stronger in the cabin environment due to merged heat loads from passengers sitting closely in the same row. Additional local airflow recirculation was found in the front of sitting passengers due to the strong interferences of cough-jets to ventilated flow and the breakup of thermal plume. Although the cough behaviour finished in half second, the effects of cough-jets could last and remain influential for at least 2 s. Due to the limited seating space in the economy cabin, the released cough flow could be locked in the local environments (i.e. near and intermediate fields) of passengers.

(2) The cough flow was found having significant effects on the residence time of cough contaminants by stimulating the contaminants travelling longer in the air. While ventilated flow started to lose its dominating influences on intermediate-size contaminants (from 50 μm to 100 μm) due to their considerable weight and inertia, the strong cough-jets still remained significant impacts on these contaminants and led to a significant increase of their residence time (up to near 50%). The cough-jets effects were gradually reduced on large-size contaminants (up to 200 μm) and became very minimal on extremely large contaminants over 500 μm.

(3) The outcomes also revealed strong impacts of cough flow on the travel characteristics of cough contaminants. Although the cough-jet did not have dominating effects on the travel displacements of contaminants, it dramatically increased the travel distances (nearly doubled) of small and intermediate sizes of contaminants (up to 200 μm). The significantly extended travel distances indicated a more severe suspensions of contaminants in passengers' local environment. Since passengers' breathing zones

were also included in their local environments, the long and severe suspension of contaminants induced by cough flow should be a critical factor to consider when conducting passengers' health-related studies in cabin environment, especially for infectious risks assessment (e.g. for the COVID-19 investigations).

(4) The cough flow was found having long and effective impacts on contaminants transport up to 4 s, which was 8 times longer than the duration of cough and contaminants release (0.5 s). Also, comparing to the ventilated flow, cough flow had considerable impacts to a much wider size range of contaminants (up to 200 μm) due to its strong jet-effects. Therefore, when investigating infectious respiratory diseases (e.g. SARS-CoV-2) transmitted via airway defensive behaviours (e.g. coughing, sneezing and speaking), it is essential to consider these strong jet-effects during the release process.

Declaration of competing interest

The authors declare that they have no known competing financial interests or personal relationships that could have appeared to influence the work reported in this paper.

Acknowledgement

The financial supports provided by the Natural Science Foundation of China (Grant No. 91643102) and Australian Research Council (Project ID: DP160101953) and Railway Manufacturing CRC of Australia (Project ID: R3.6.1) are gratefully acknowledged.

References

[1] J. Hiscott, M. Alexandridi, M. Muscolini, E. Tassone, E. Palermo, M. Soultsioti, A. Zevini, The Global Impact of the Coronavirus Pandemic, Cytokine Growth Factor Rev, 2020.
[2] The Department of Health Australian, National Framework for Communicable Disease Control, Australian Government Department of Health, Commonwealth of Australia, 2014.
[3] Coronavirus Resource Center, COVID-19 dashboard by the center for systems science and engineering (CSSE) at Johns Hopkins university (JHU). https://coronavirus.jhu.edu/map.html, 2020. (Accessed 15 June 2020).
[4] M. Saez, A. Tobias, D. Varga, M.A. Barcelo, Effectiveness of the measures to flatten the epidemic curve of COVID-19. The case of Spain, Sci. Total Environ. 727 (2020) 138761.
[5] S.M. Iacus, F. Natale, C. Santamaria, S. Spyratos, M. Vespe, Estimating and projecting air passenger Traffic during the COVID-19 coronavirus outbreak and its socio-economic impact, Saf. Sci. (2020) 104791.
[6] World Health Organisation, Novel Coronavirus(2019-nCoV) - Situation Report World Health Organisation, 2020.
[7] J.M. Read, J.R.E. Bridgen, D.A.T. Cummings, A. Ho, C.P. Jewell, Novel Coronavirus 2019-nCoV: Early Estimation of Epidemiological Parameters and Epidemic Predictions, medRxiv (2020), 2020, 01.23.20018549.
[8] Y. Liu, A.A. Gayle, A. Wilder-Smith, J. Rocklöv, The reproductive number of COVID-19 is higher compared to SARS coronavirus, J. Trav. Med. 27 (2) (2020).
[9] Q. Li, X. Guan, P. Wu, X. Wang, L. Zhou, Y. Tong, R. Ren, K.S.M. Leung, E.H.Y. Lau, J.Y. Wong, X. Xing, N. Xiang, Y. Wu, C. Li, Q. Chen, D. Li, T. Liu, J. Zhao, M. Liu, W. Tu, C. Chen, L. Jin, R. Yang, Q. Wang, S. Zhou, R. Wang, H. Liu, Y. Luo, Y. Liu, G. Shao, H. Li, Z. Tao, Y. Yang, Z. Deng, B. Liu, Z. Ma, Y. Zhang, G. Shi, T.T.Y. Lam, J.T. Wu, G.F. Gao, B.J. Cowling, B. Yang, G.M. Leung, Z. Feng, Early transmission dynamics in Wuhan, China, of novel coronavirus–infected Pneumonia, N. Engl. J. Med. 382 (13) (2020) 1199–1207.
[10] F.R. Lirong Zou, Mingxing Huang, Lijun Liang, Huitao Huang, Zhongsi Hong, Jianxiang Yu, Min Kang, Yingchao Song, Jinyu Xia, Qianfang Guo, Tie Song, Jianfeng He, Hui-Ling yen, Malik Peiris, Jie Wu, SARS-CoV-2 Viral Load in Upper Respiratory Specimens of Infected Patients, 2020.
[11] Y. Yan, X. Li, Y. Shang, J. Tu, Evaluation of airborne disease infection risks in an airliner cabin using the Lagrangian-based Wells-Riley approach, Build. Environ. 121 (2017) 79–92.
[12] J.K. Gupta, C.H. Lin, Q. Chen, Transport of expiratory droplets in an aircraft cabin, Indoor Air 21 (1) (2011) 3–11.
[13] G.Q. Qian, N.B. Yang, F. Ding, A.H.Y. Ma, Z.Y. Wang, Y.F. Shen, C.W. Shi, X. Lian, J.G. Chu, L. Chen, Z.Y. Wang, D.W. Ren, G.X. Li, X.Q. Chen, H.J. Shen, X.M. Chen, Epidemiologic and clinical characteristics of 91 hospitalized patients with COVID-19 in Zhejiang, China: a retrospective, multi-centre case series, QJM, Int. J. Med. (2020).
[14] N. Yang, Y. Shen, C. Shi, A.H.Y. Ma, X. Zhang, X. Jian, L. Wang, J. Shi, C. Wu, G. Li, Y. Fu, K. Wang, M. Lu, G. Qian, In-flight Transmission Cluster of COVID-19: A Retrospective Case Series, medmRxiv, 2020, p. 2020, 03.28.20040097.
[15] S. Park, R.T. Hellwig, G. Grün, A. Holm, Local and overall thermal comfort in an aircraft cabin and their interrelations, Build. Environ. 46 (5) (2011) 1056–1064.
[16] R.K. Dygert, T.Q. Dang, Experimental validation of local exhaust strategies for improved IAQ in aircraft cabins, Build. Environ. 47 (2012) 76–88.
[17] R.K. Dygert, T.Q. Dang, Mitigation of cross-contamination in an aircraft cabin via localized exhaust, Build. Environ. 45 (9) (2010) 2015–2026.
[18] J. Li, X. Cao, J. Liu, C. Wang, Y. Zhang, Global airflow field distribution in a cabin mock-up measured via large-scale 2D-PIV, Build. Environ. 93 (2015) 234–244.
[19] M. Li, B. Zhao, J. Tu, Y. Yan, Study on the carbon dioxide lockup phenomenon in aircraft cabin by computational fluid dynamics, Build Simu 8 (4) (2015) 431–441.
[20] Y. Yan, X. Li, J. Tu, Effects of passenger thermal plume on the transport and distribution characteristics of airborne particles in an airliner cabin section, Sci. Tech. Built Environ. 22 (2) (2015) 153–163.
[21] S. Liu, L. Xu, J. Chao, C. Shen, J. Liu, H. Sun, X. Xiao, G. Nan, Thermal environment around passengers in an aircraft cabin, HVAC R Res. 19 (5) (2013) 627–634.
[22] S.B. Poussou, S. Mazumdar, M.W. Plesniak, P.E. Sojka, Q. Chen, Flow and contaminant transport in an airliner cabin induced by a moving body: model experiments and CFD predictions, Atmos. Environ. 44 (24) (2010) 2830–2839.
[23] Z. Han, G.N.S. To, S.C. Fu, C.Y. Chao, W. Weng, Q. Huang, Effect of human movement on airborne disease transmission in an airplane cabin: study using numerical modeling and quantitative risk analysis, BMC Infect. Dis. 14 (434) (2014).
[24] S.S. Isukapalli, S. Mazumdar, P. George, B. Wei, B. Jones, C.P. Weisel, Computational fluid dynamics modeling of transport and deposition of pesticides in an aircraft cabin, Atmos. Environ. 68 (2013) 198–207.
[25] L. Bourouiba, E. Dehandschoewercker, John W.M. Bush, Violent expiratory events: on coughing and sneezing, J. Fluid Mech. 745 (2014) 537–563.
[26] M.D. Anwarul Hasan, C.F. Lange, M.L. King, Effect of artificial mucus properties on the characteristics of airborne bioaerosol droplets generated during simulated coughing, J. Non-Newtonian Fluid Mech. 165 (21) (2010) 1431–1441.
[27] S.B. Kwon, J. Park, J. Jang, Y. Cho, D.S. Park, C. Kim, G.N. Bae, A. Jang, Study on the initial velocity distribution of exhaled air from coughing and speaking, Chemosphere 87 (11) (2012) 1260–1264.
[28] Y. Yan, X. Li, L. Yang, J. Tu, Evaluation of manikin simplification methods for CFD simulations in occupied indoor environments, Energy Build. 127 (2016) 611–626.
[29] X. Li, Y. Yan, J. Tu, The simplification of computer simulated persons (CSPs) in CFD models of occupied indoor spaces, Build. Environ. 93 (2015) 155–164.
[30] ANSYS®, Academic Research Release 19.2, Help System, Coupled Field Analysis Guide, ANSYS, Inc., 2019.
[31] R.J. Roache, Perspective A method for uniform reporting of grid refinement studies, J. Fluid Eng. 116 (1994) 405–413.
[32] Q. Chen, Comparison of different k-ε models for indoor air flow computations, Numer Heat Tr B-Fund 28 (3) (1995) 353–369.
[33] M. Li, Y. Yan, B. Zhao, J. Tu, J. Liu, F. Li, C. Wang, Assessment of turbulence models and air supply opening models for CFD modelling of airflow and gaseous contaminant distributions in aircraft cabins, Indoor Built Environ. (2017), 1420326X1668804.
[34] W. Liu, J. Wen, J. Chao, W. Yin, C. Shen, D. Lai, C.-H. Lin, J. Liu, H. Sun, Q. Chen, Accurate and high-resolution boundary conditions and flow fields in the first-class cabin of an MD-82 commercial airliner, Atmos. Environ. 56 (2012) 33–44.
[35] ASHRAE, ANSI/ASHRAE Standard 161-2013, Air Quality within Commercial Aircraft, ASHRAE, Atlanta, GA, 2013.
[36] R.J. deDear, E. Arens, Z. Hui, M. Oguro, Convective and radiative heat transfer coefficients for individual human body segments, Int. J. Biometeorol. 40 (3) (1997) 141–156.
[37] D. Licina, J. Pantelic, A. Melikov, C. Sekhar, K.W. Tham, Experimental investigation of the human convective boundary layer in a quiescent indoor environment, Build. Environ. 75 (2014) 79–91.
[38] J.K. Gupta, C.H. Lin, Q. Chen, Flow dynamics and characterization of a cough, Indoor Air 19 (6) (2009) 517–525.
[39] H. Fellouah, C.G. Ball, A. Pollard, Reynolds number effects within the development region of a turbulent round free jet, Int. J. Heat Mass Tran. 52 (17–18) (2009) 3943–3954.
[40] J.K. Gupta, C.H. Lin, Q. Chen, Flow dynamics and characterization of a cough, Indoor Air 19 (6) (2009) 517–525.
[41] J. Wei, Y. Li, Human cough as a two-stage jet and its role in particle transport, PloS One 12 (1) (2017), e0169235.